Computational Study on 4-Amino-3-Hydroxynaphthalene-1-sulfonic Acid (AHNSA)

ABSTRACT

A computational study on 4-amino-3-hydroxynaphthalene-1-sulfonic acid (AHNSA) has been carried out to investigate formation of poly-(AHNSA), and to obtain binding structures and energies of AHNSA-Ephedrine and AHNSA-Caffeine complexes. For this purpose, the DFT/B3LYP/6-31G(D) and DFT/B3LYP/6-31+G(D) level of theories were utilized. These were investigated from analysis of their atomic charge distributions, total spin density, frontier molecular orbitals, electrostatic potential maps and calculations of binding energies. Results from analysis suggest that homo-polymerization of AHNSA should involve the molecular orbitals arising between radical cations formed from the neutral monomer. The resulting data illustrated that the method was likely to be useful for homo-polymerization of AHNSA. Calculated binding energies of AHNSA-Caffeine and AHNSA-Ephedrine complexes were -8.77 kcal mol^{-1} and -8.36 kcal mol^{-1}, respectively, which indicated that both complexes could be formed.

Keywords: *4-Amino-3-Hydroxynaphthalene-1-sulfonic Acid, DFT, Binding energy*

1. Introduction

Polymer modified electrodes (PMEs) have received attention in recent years due to their good stability, reproducibility, increase in active sites, homogeneity in electrochemical deposition and strong adherence to electrode surfaces [1-4]. Polyaniline is one of the most studied conducting polymers used as electrochemical sensors [5, 6].

4-Amino-3-hydroxynaphthalene-1-sulfonic acid (AHNSA) is a derivative of aniline with trifunctional monomer, i.e. bearing three functional groups ($–NH_2$, –OH and $–SO_3H$), and contains two fused benzene rings, of which ($–NH_2$ and –OH) may take part in the polymerization, depending on the nature of the reaction medium.[7].

Marjanovic et al. [8] reported the electrochemical oxidative polymerization and structural characterization of sodium 4-amino-3-hydroxynaphthalene-1-sulfonate. They found that polymerization occurred selectively *via* amino groups, and that hydroxyl groups were unaffected during polymerization. Marjanovic et al. [9] also reported the chemical oxidative polymerization of 4-amino-3-hydroxynaphthalene-1-sulfonate in different media like hydrochloride and mono- and disodium salts. They studied the naphthalene oxide-type structure only in the case of the disodium salt.

Poly-(AHNSA) belongs to a group of very stable conducting polymers and has been synthesized electrochemically on different electrode surfaces, mainly glassy carbon. Poly-(AHNSA) has high electrical conductivity and high chemical stability in aqueous solutions. Poly (4-amino-3-hydroxynaphthalene sulfonic acid)-modified glassy carbon electrode has been developed as fast, simple method for quantitative determination of caffeine in coffee and Ephedrine in human urine was reported [10, 11].

A survey of the scientific literature shows that only a spectral properties computational study of 4-amino-3-hydroxynaphthalene-1-sulfonic acid was conducted by Sebastian, et al.[12]. A more detailed computational study of AHNSA is therefore warranted to elucidate additional molecular properties of AHNSA.

In this work the geometrical parameters, atomic charge and spin density distribution, Frontier Molecular Orbital (FMO) analysis and Map of Electrostatic Potential (MEP) of AHNSA were calculated using DFT method to investigate its polymerization and compare the outcomes with the experimental results reported in References [10,11]. In addition, binding energies of AHNSA-Ephedrine and AHNSA -Caffeine complexes were investigated to confirm the stability of the complexes.

2. COMPUTATIONAL DETAILS

All calculations were carried out with the Gaussian 09W program package [13].The visualization of result was made possible by using Gaussian view 5.0.8[14].The geometry of all species were optimized at DFT/ 6-31G(d) and 6-31+G(d) levels of theory with the Becke's gradient-corrected exchange-functional, as well the hybrid three-parameter (B3) in conjunction with the Lee, Yang, and Parr (LYP) correlation functional, i.e., at a B3LYP as a function of the basis set, using default symmetry constraint [15, 16]. The calculations on the AHNSA radical cation were done under unrestricted condition. The geometry optimization of the neutral monomers and radical cations was considered complete when a stationary point was found. The optimized structures were used to calculate the properties of the neutral monomer and the corresponding radical cation formed under acidic and basic conditions.

Ground state and FMO energies of the monomers and radical cations are reported at the B3LYP/6-31G(d) level of theory. The effective atomic charges were estimated by Mulliken population analysis, although atomic net spin population has its own limitations, using the same basis set and level of theory. Unpaired electron spin density distribution in the radical cation was calculated at the UB3LYP/6-31G(d) and UB3LYP/6-31+G(d). The molecular electrostatic potential map was also analyzed.

In addition, geometries of the studied complexes were optimized using B3LYP with6-31G(d) basis sets, which are known to yield good geometry parameters at a moderate computational cost [17]. Binding energy values of the complexes were determined using optimized geometry of the complexes by DFT/ B3LYP method with 6-31G (d) basis sets.

3. RESULTS AND DISCUSSION

3.1 Geometry Optimizations

The geometrical parameters of AHNSA (Fig.1) are listed in Table 1. The molecular structure with numbering adopted in this study is shown in Scheme 1. Scheme 2 depicts the structures of species considered in this study.

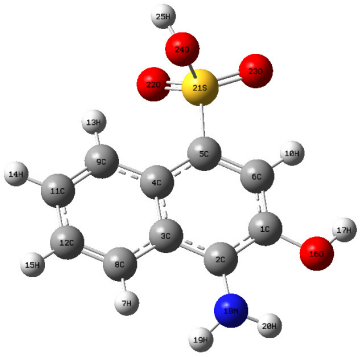

Figure 1: Optimized structure of AHNSA

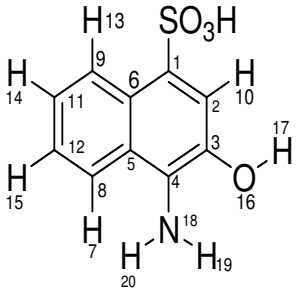

Scheme 1: Molecular structure and numbering scheme of AHNSA

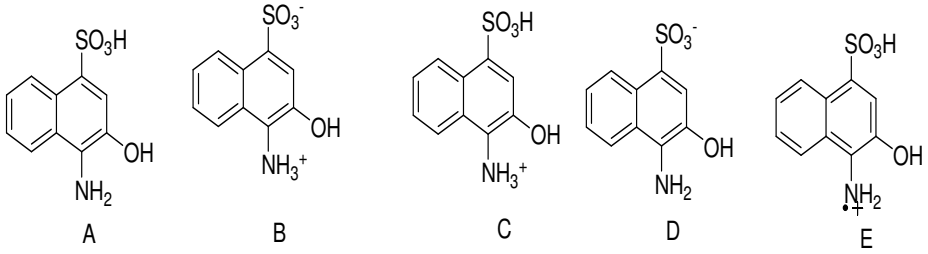

Scheme 2: Structures used to model **A**) AHNSA, **B**) zwitterionic AHNSA, **C**) protonated AHNSA, **D**) deprotonated AHNSA, and **E**) AHNSA radical cation

Structures a) and b) are found in neutral conditions, c) and d) are found in acidic and basic medium respectively, and structure e) is found through a comproportonation reaction.

Table 1: Bond length (Å), bond angle (°) and torsion angle for the neutral AHNSA calculated using DFT (B3LYP/6-31G(d)) and (B3LYP/6-31+G(d)) methodologies.

Parameters	Basis set used		Reference 12	parameters	Basis set used		Reference 12
Bond length(Å)	B3LYP/ 6-31G(d)	B3LYP/ 6-31+G(d)	B3LYP/ 6-31G(d, p)	Bond angle (°)	B3LYP/ 6-31G(d)	B3LYP/ 6-31+G(d)	B3LYP/ 6-1G(d, p)
R(C3,C4)	1.395	1.394	1.394	A(C4,C3,C2)	121.05	121.25	121.20
R(C3,C2)	1.397	1.397	1.399	A(C4,C3,O16)	116.17	116.08	116.16
R(C3,O16)	1.377	1.379	1.376	A(C2,C3,O16)	122.78	122.66	122.63
R(C4,C5)	1.432	1.434	1.431	A(C3,C4,C5)	119.16	119.05	118.99
R(C4,N18)	1.385	1.383	1.385	A(C3,C4,N18)	118.84	118.77	119.01
R(C5,C6)	1.438	1.439	1.438	A(C5,C4,N18)	121.96	122.12	121.96
R(C5,C8)	1.421	1.422	1.422	A(C4,C5,C6)	120.29	120.29	120.32
R(C1,C6)	1.428	1.429	1.428	A (C4,C5,C8)	120.91	120.98	120.89
R(C6,C9)	1.422	1.423	1.423	A(C6,C5,C8)	118.80	118.73	118.78
R(C1,C2)	1.385	1.385	1.384	A(C5,C6,C1)	117.52	117.50	117.75
R(C1,S21)	1.775	1.778	1.788	A(C5,C6,C9)	118.32	118.35	118.27
R(C8,C12)	1.376	1.378	1.375	A(C1,C6,C9)	124.16	124.15	123.98
R(C9,C11)	1.376	1.378	1.375	A(C6,C1,C2)	121.33	121.39	121.03
R(C11,C12)	1.412	1.413	1.412	A(C6,C1,S21)	123.14	123.17	120.44
RS(21,O22)	1.466	1.467	1.466	A(C2,C1,S21)	115.53	115.44	118.28
R(S21,O23)	1.461	1.463	1.456	A(C3,C2,C1)	120.60	120.48	120.64
R(S21,O24)	1.652	1.657	1.652	A(C5,C8,C12)	121.25	121.34	121.29
A(C1,S21,O22)	112.30	112.563	110.19	A(C6,C9,C11)	121.13	121.20	121.17
A(C1,S21,O23)	108.95	108.9	110.32	A(C9,C11,C12)	120.54	120.48	120.53
A(C1,S21,O24)	99.16	99.17	101.66	A (O23,S21,O24)	108.70	108.46	106.17
A(O22,S21,O23)	119.33	119.32	120.74	A(C8,C12,C11)	119.91	119.89	119.93
A(O22,S21,O24)	106.40	106.36	105.83				

The AHNSA molecule has eleven C–C, three S–O, two O–H, two N–H, five C–H, one C–O, one C–S and one C–N bonds, the C–C bonds in naphthalene ring are not of the same length. This is due to the fact that the electron donating (NH_2, O–H) groups and electron withdrawing (-SO_3H) group

on the naphthalene ring tends to contract and elongate the C–C bond lengths adjacent to the substituent, as displayed in Table 1. The bond lengths are slightly increased in order C8–C12 = C9-C11= 1.376 Å, C2-C3= 1.385 Å, C3–C4 = 1.395 Å, C2-C3=1.397, C11–C12 = 1.412 Å, C5–C8 = 1.421 Å, C6–C9 = 1.422 Å,C1–C6 = 1.428 Å, C4–C5 = 1.432 Å, and C5–C6 = 1.438 Å where as C1–C2 = 1.375 Å, C5–C6 = 1.375 Å, C9–C14 = 1.394 Å, C10–C13 = 1.384 Å, C13–C14 = 1.399 Å are decreased, in order respectively as shown in Table 1.

The computed bond lengths for S21–O22 = 1.466 Å, S21–O23 = 1.461 Å and S21–O24 = 1.652 Å, the bond length S21–O24 = 1.652 Å shows that it is a pure single bond character. The C–N18 bond length is found to be 1.385 Å and that of C–S21 is 1.775 Å by B3LYP/6-31G(d, p) method which is almost similar to our computations with B3LYP/6-31G(d) and B3LYP/6-31+G(d) methods.

From our results, the combination of the hybrid functional B3LYP and the 6-31G(d) atomic basis set was sufficient to warrant an acceptable computational cost to perform the calculations, as it can be seen in Table 1.

The naphthalene ring appears slightly distorted as expected due to the presence of electron donating and electron withdrawing groups. This is evident from the computed endocyclic bond angles, which increase in order of C5-C6-C1=117.52°, C3-C4-C5=119.16°, C4-C5-C6=120.29°, C1-C2-C3=120.60°, C4-C5-C8=120.91°, C2-C3-C4=121.05°, C6-C1-C2=121.33°, C1-C6-C9=124.16.52°, C5-C6-C1=117.52°, C5-C6-C1=117.52°and C5-C6-C1=117.52° as shown in Table 1.

Table 2: Optimized bond length (Å) of AHNSA and AHNSACR in acidic and basic medium calculated at the B3LYP/6-31G(d) level.

Bond length (Å)	**AHNSA**	**AHNSACR**	**Bipolar AHNSA**	**Protonated AHNSA**	**Protonated AHNSACR**	**Deprotonated AHNSA**
R(C1-S21)	1.7752	1.8131	1.7676	1.8029	1.8183	1.8104
R(C3-O16)	1.3766	1.3399	1.3722	1.3531	1.3194	1.3768

R(C4-N18)	1.3845	1.3345	1.379	1.4738	1.4693	1.4004
R(S-O22)	1.4658	1.4513	1.4695	1.4631	1.4586	1.4935
R(S=O23)	1.4613	1.4575	1.4657	1.4585	1.4538	1.4924
R(S=O24)	1.654	1.6344	1.6445	1.628 0	1.6155	1.4935
R(SO24-H25)	0.9774	0.9792	--	0.9792	0.9808	--

The optimized bond lengths for the AHNSA and its corresponding radicals under acidic and basic condition are collected in Table 2. The formation of radical cation **E** results in shortening of C3-O16 by 0.037 and C4-N18 by 0.05. The shortening in bond length indicates contribution of heteroatom to the resonance of the aromatic ring.

3.2 Charge and Spin Distribution Analysis

3.2.1 Atomic Charge Distribution

Using Mulliken population analysis, the net atomic charges of different form of AHNSA and its radical cation were calculated to find out where the atomic charges will be preferentially localized.

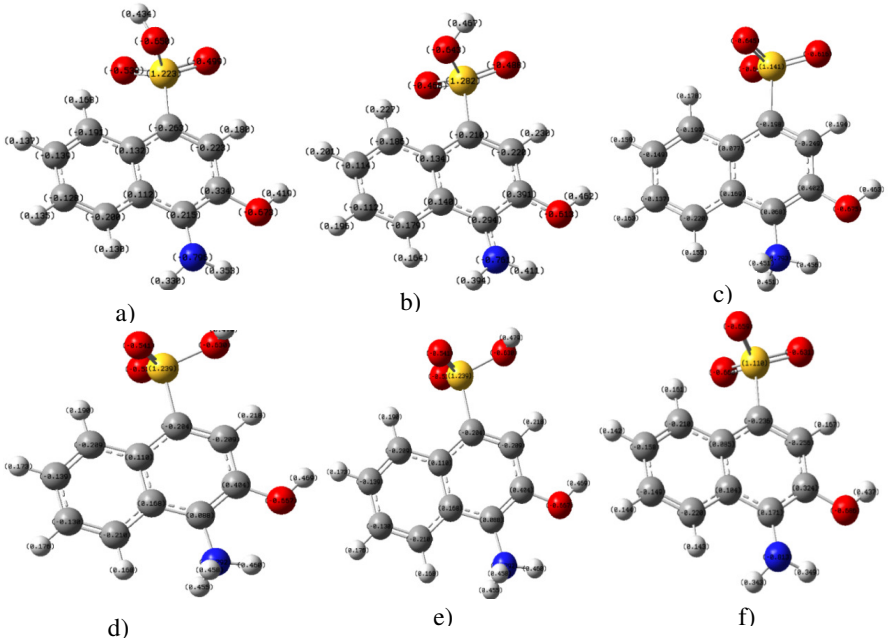

Figure 2: Atomic charge distribution in a) AHNSA, b) AHNSACR, c) bipolar AHNSA, d) protonated AHNSA, e) protonated AHNSACR, and f) deprotonated AHNSA calculated at B3LYP/6-31G(d) level

The atomic charge distributions data obtained from optimized structures in Figure 2. are collected in Table 3.

Table 3: Atomic charge distribution in AHNSA, AHNSACR, bipolar AHNSA, protonated AHNSA, protonated AHNSACR, and deprotonated AHNSA calculated at B3LYP/6-31G(d) level .

Atoms	**AHNSA**	**AHNSACR**	**Bipolar AHNSA**	**Protonated AHNSA**	**Protonated AHNSACR**	**Deprotonated AHNSA**
C1	-0.262916	-0.209783	-0.272427	-0.204390	-0.163617	-0.236211

C2	-0.222596	-0.220406	-0.219180	-0.208652	-0.176604	-0.256443
C3	0.333700	0.390863	0.329041	0.404104	0.470187	0.324457
C4	0.214839	0.293863	0.216318	0.087563	0.139207	0.170586
C5	0.111985	0.140046	0.100938	0.167629	0.187565	0.104338
C6	0.131517	0.133999	0.130546	0.109916	0.137310	0.084582
C8	-0.200490	-0.179048	-0.209805	-0.209733	-0.126318	-0.220156
C9	-0.190727	-0.185636	-0.211111	-0.209421	-0.171926	-0.209883
C11	-0.139458	-0.114183	-0.149917	-0.139132	-0.076748	-0.158278
C12	-0.128473	-0.111794	-0.143688	-0.129983	-0.102105	-0.149108
N	-0.796176	-0.761014	-0.807962	-0.792423	-0.794201	-0.812555
S	1.222667	1.282404	1.215567	1.238825	1.270124	1.110052
O16	-0.673317	-0.673317	-0.679742	-0.666978	-0.593925	-0.686141
O22	-0.537649	-0.467787	-0.565489	-0.540766	-0.516003	-0.659995
O23	-0.498981	-0.488404	-0.528312	-0.522863	-0.488341	-0.631255
O24	-0.649608	-0.642648	-0.660863	-0.629815	-0.614214	-0.659409

As we observe from table 3 above, for all species in the table, the nitrogen charge is more negative than oxygen. Thus, in the formation of AHNSACR, an electron is expected to be removed from a lone pair of the nitrogen. This confirms that the *–OH* group will remain unaffected, which leads to a nitrogen linkage for the formation of poly(AHNSA).

AHNSA radicals are generated *via* a comproportionation reaction between AHNSA and its oxidized form obtained by two-electron oxidation, rather than by the one-electron anodic oxidation of the monomer [9].

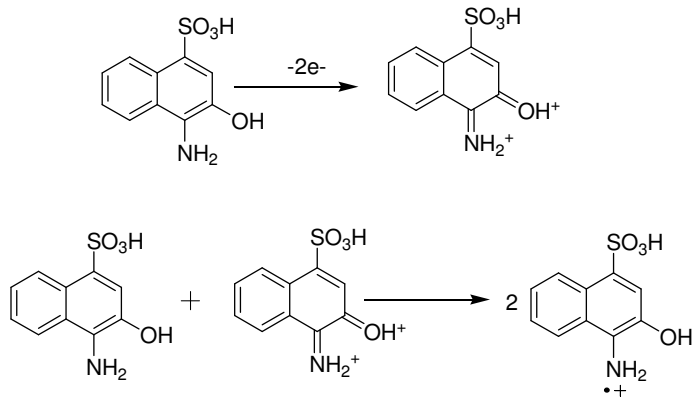

Scheme 3: Proposed mechanism for formation of AHNSACR *via* comproportionation redox reaction.

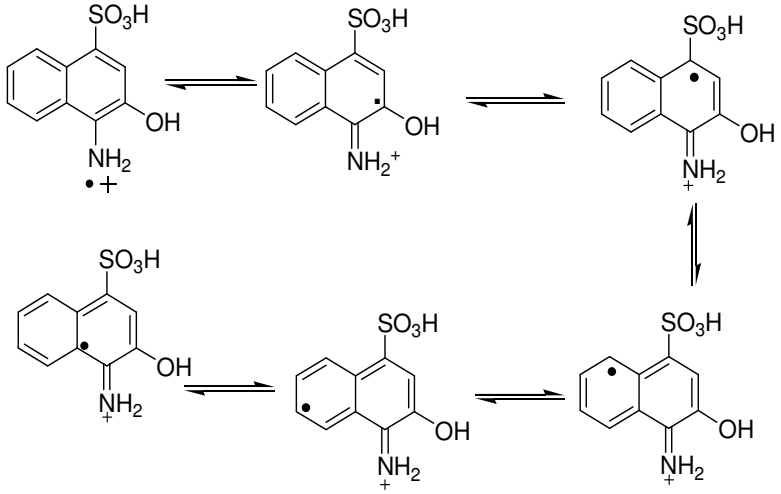

Scheme 4: Pictorial representation of spin density delocalization of AHNSACR.

Once the AHNSACR formed, DFT B3LYP/ 6-31G(d) calculations show that the electron of the AHNSACR is delocalized mainly over the substituted fused benzene ring (excluding C2 and C11) and the nitrogen.

3.2.2 Spin Density Distribution of AHNSACR

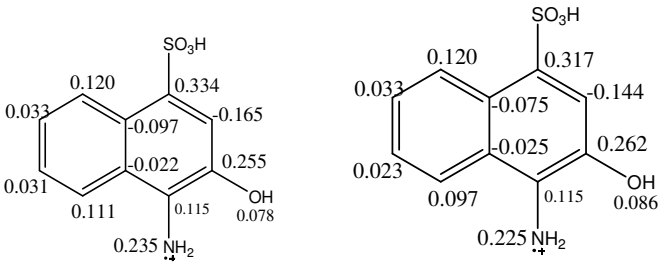

Scheme 5: Total Spin densities distribution of AHNSACR calculated at: **A**) B3LYP/ 6-31G(d) and **B**) B3LYP/ 6-31G(d) levels

The highest spin densities are observed at C1(0.334), C3(0.255), N(0.235), C9(0.120) and C4(0.115) of AHNSACR. In contrast, low spin densities are obtained at C5(-0.022) and C6(-0.097) of the naphthalene ring (Scheme 5 (**A**). For examining the initiating and propagating reactions, it is reasonable to assume that coupling reactions preferentially occurred between carbons having higher spin densities [18]. But C1, C3 and C4 sites are sterically hindered and the possible sites for coupling reaction are C9 and N. These facts indicate that in coupling, the possible sites for the propagation reaction of the radical cation can be realized from C9 and N. The spin density of the nitrogen (0.235) is much higher than that of the hydroxyl oxygen (0.078). Hence, it can be concluded that aromatic amine oxidative polymerization dominates over phenol oxidative polymerization, as found experimentally [19].

3.3 Frontier molecular orbital (FMO) analysis

Frontier orbital theory suggests a simple way of interpreting acid conjugated base reaction. The Frontier Molecular Orbital (FMO) pictures of the monomer (Highest Occupied Molecular Orbital, HOMO, and Lowest Unoccupied Molecular Orbital, LUMO) of different forms of AHNSA shown in Figure 3 and HOMO-LUMO energies and their gaps are presented in Table 4.

The HOMO-LUMO pairs that are closer together in energy will interact more strongly. The radical cation can be generated by the removal of a single electron from the HOMO. This leads to the formation of two Singly Occupied Molecular Orbitals, SOMO-α and SOMO-β, where α and β represent opposite spin of electrons. After radical cation formation, the coupling reaction is expected to occur between two nearly identical SOMOs in the radical-radical coupling model or between HOMO - SOMO in the monomer-radical coupling mode. The diagram in Figure 3 below represents these orbitals.

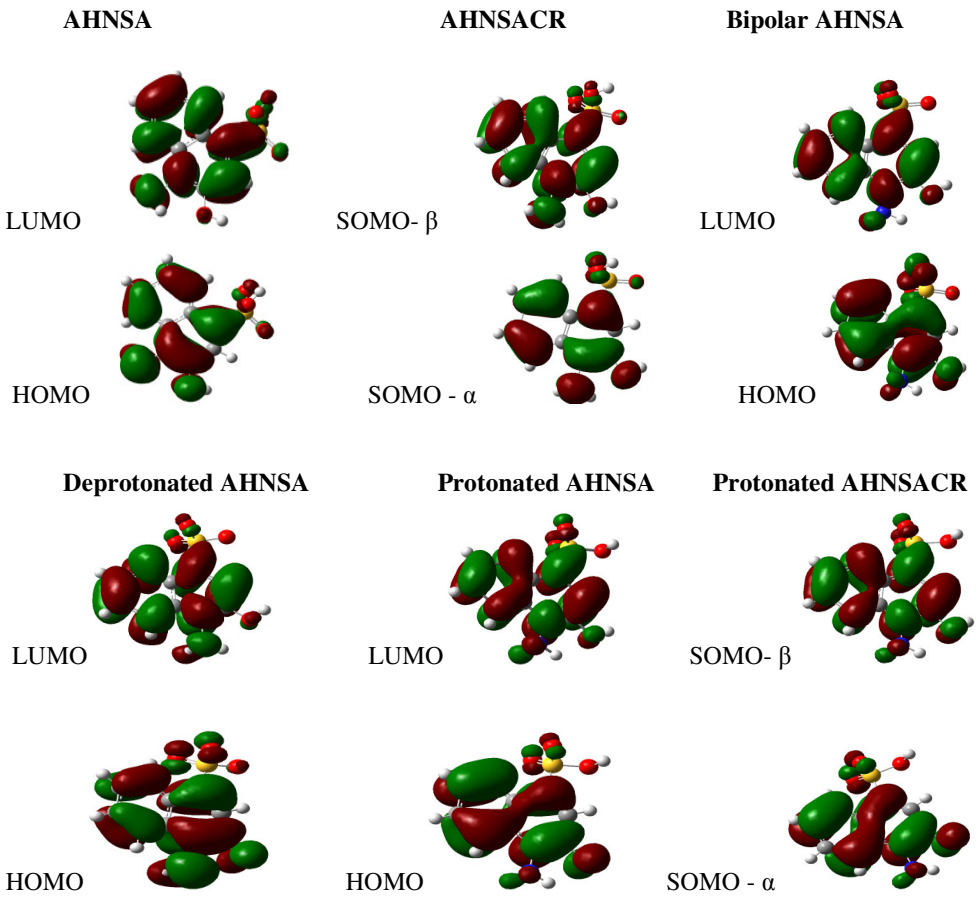

Figure 3: Schematic representation of different forms AHNSA orbitals involved in the coupling calculated at B3LYP/6-31G(d) level of theory, within a 0.02 isosurface cutoff approximation

Table 4: The HOMO-LUMO energies and their energy gaps of different forms of AHNSA.

Energy	AHNSA	AHNSACR (SOMO)	Bipolar AHNSA	Deprotonated AHNSA	Protonated AHNSA	Protonated AHNSACR
E_{LUMO}(eV)	-1.496	-10.1896 (β)	-1.7608	-0.9608	-2.3435	-8.1348 (β)
E_{HOMO}(eV)	-5.523	-11.0927 (α)	-6.3011	-5.0548	-6.7460	-8.4668 (α)
E_{LUMO}-E_{HOMO} (eV)	4.027	0.903	4.540	4.094	4.403	0.332

From the values for the HOMO-LUMO energies and their energy gaps summarized in Table 4, it can be seen that among the species presented, the AHNSACR SOMO-α (-11.0927eV) and SOMO-β(-10.1896eV) are stable species and their small energy gap (0.903eV) indicates that the SOMO-α - SOMO- β of the AHNSACR are involved in coupling reaction.

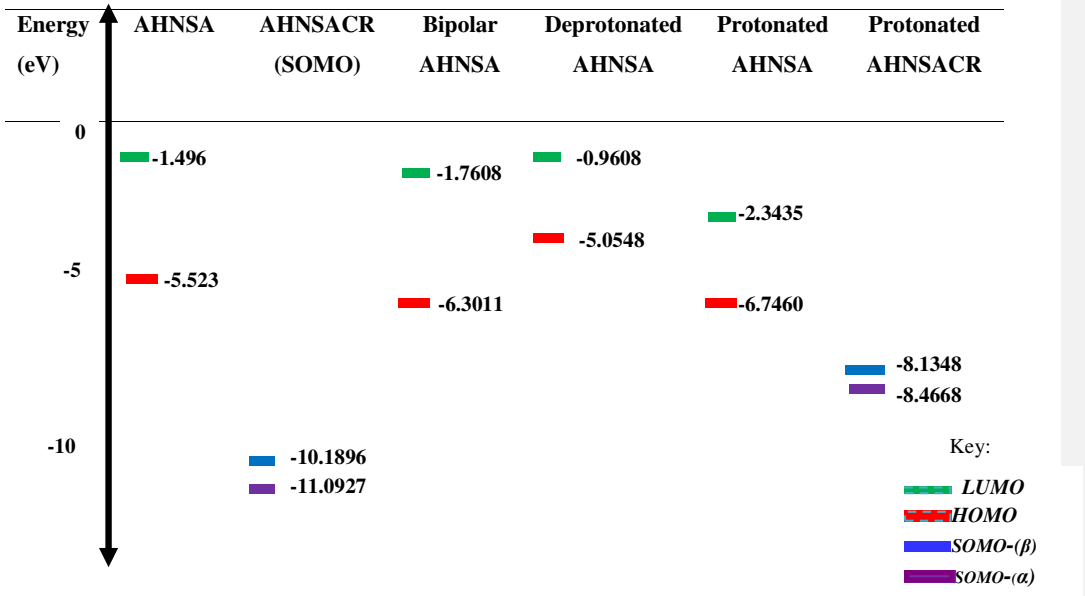

Figure 4: Energy diagram and illustrations of AHNSA, AHNSACR, bipolar AHNSA, deprotonated AHNSA, protonated AHNSA, and protonated AHNSACR molecular orbitals, obtained using DFT/(B3LYP/6-31G(d)) methodology within a 0.02 isosurface cutoff approximation.

As shown in the energy diagram of Figure 4, the lowering energy of SOMO after radical cation formation implies removal of an electron is favorable and the radical cation is stable compared to other species presented in energy diagram of Figure 4. In addition, it can be observed that the AHNSACR, SOMO-α and SOMO-β are the pair closer together in energy and their energy gap is small, hence the radical-radical coupling mode is a likely pathway for electropoymerization of AHNSA. For AHNSACR, the occupancy of the unpaired electron of SOMO is on the amino group.

Comment [JCS1]: electropolymerization

To complement the information obtained from atomic charge distribution, the unpaired electron spin density distribution, and FMO analysis, the electrostatic potential map of the radical cations have been evaluated.

3.4 Electrostatic potential map analysis

Electrostatic potential maps can be used to analyze charge distributions in compounds. The molecular electrostatic potential (MEP) surfaces show the electrophilic / nucleophilic sites of the molecules. The resulting molecular electrostatic potential surface mapped in terms of color grading, RED < ORANGE < YELLOW < GREEN < BLUE. The more red an area is, the higher the electron density, and the more blue an area is, the lower the electron density. The variation in electrostatic potential is largely responsible for identifying binding sites in a molecule.

To predict the reactive sites for electrophilic and nucleophilic attack for AHNSA, the MEP at the B3LYP/6-31G(d) method was calculated.

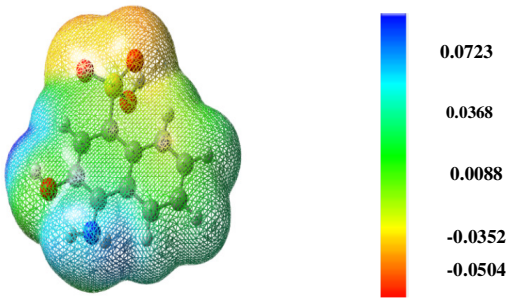

Figure 5: Molecular Electrostatic Potential (MEP) surface of AHNSA calculated at the B3LYP/ 6-31G(d)method.

The color code of the map in Figure 5 ranges between -0.0504 (light red) a.u. to 0.0723 a.u. (deep blue). This indicates, the region having the positive potential are over the ring and amino hydrogen's. All these molecular properties presented above show the way in which AHNSA can be homo-polymerized.

Comment [JCS2]: should be a.u.

3.5 Coupling mechanisms

3.5.1 Radical-radical coupling

Generated *via* a comproportionation redox process, the AHNSA radicals instantaneously react among themselves, and radical–radical couplings lead to dimeric intermediates. These intermediates then lose two protons, generating dimer products (Schemes 6 and 7), which are further oxidized to radicals. This allows radical–radical coupling to continue, and polymerization to progress to completion.

As explained in Reference [9], we based our prediction of dominant AHNSA coupling reactions on the stability of the AHNSA dimeric intermediates, resembling structurally the transition state of the AHNSA radical recombination, rather than on the stability of the AHNSA dimers. As the analysis of total spin densities indicates, radical-radical coupling of AHNSACR are the possible way of polymerization. Therefore, the possible sites which have high spins are Nitrogen and C9, leaving C1, C3, and C4 due to steric hindrance.

Nitrogen-Nitrogen (N-N) coupling

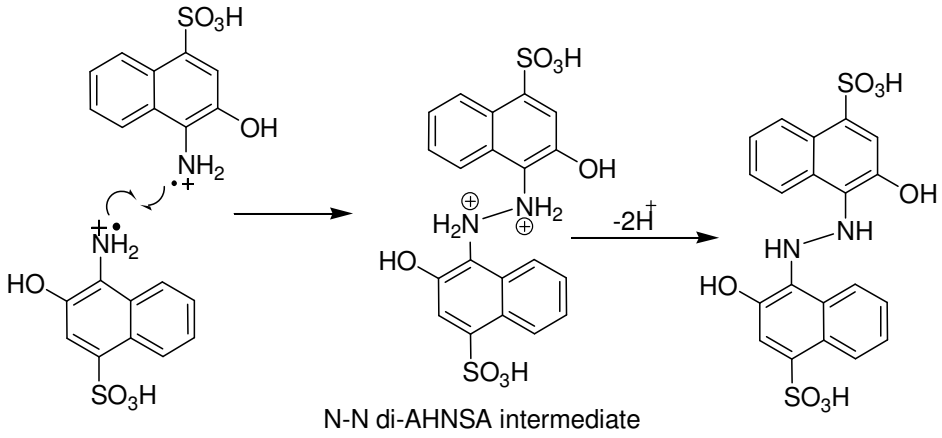

Scheme 6: Proposed polymerization Mechanism for AHNSA through N-N coupling reactions

Nitrogen-Carbon (N-C9) coupling

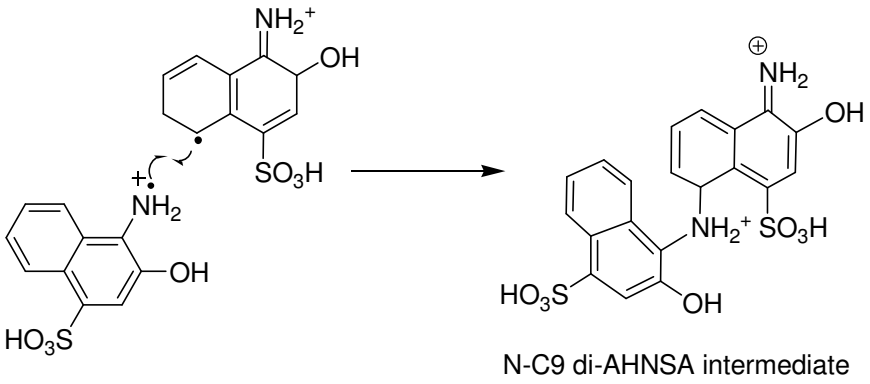

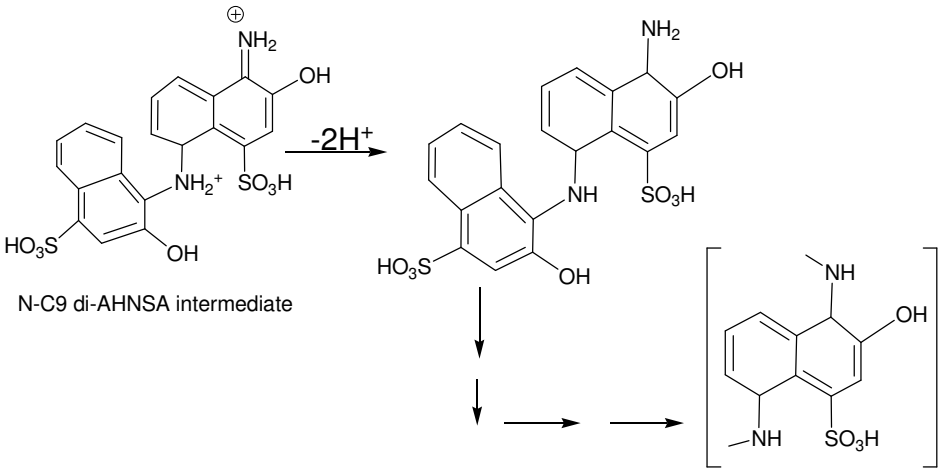

Scheme 7: Proposed polymerization Mechanism for AHNSA through N-C9 coupling reactions

Thus, based on results from our study of spin density distribution in resonance forms of AHNSACR (Scheme 4), physical observation of AHNSACR structures to account for steric repulsions during dimerization, and Scheme 6, the N–C9 coupled intermediate is a more stable transitional intermediate than the N-N coupled intermediate for the formation of poly(-AHNSA). Good agreement between theoretically predicted and experimentally determined coupling modes has been found.

3.6 Interactions of AHNSA with Ephedrine and Caffeine

3.6.1 Chemical Structures and Optimizations of Caffeine and Ephedrine

The structures in Figures 6 – 8, were employed in geometry optimization for binding energies analysis of AHNSA-Ephedrine and AHNSA-Caffeine complexes. The results are compiled in Table5.

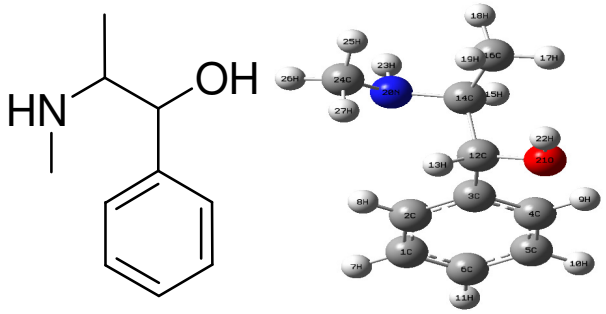

a) b)

Figure 6: **A**) Chemical structure used to model Ephedrine, **B**) optimized structure of ephedrine at B3LYP/6-31G(d) level.

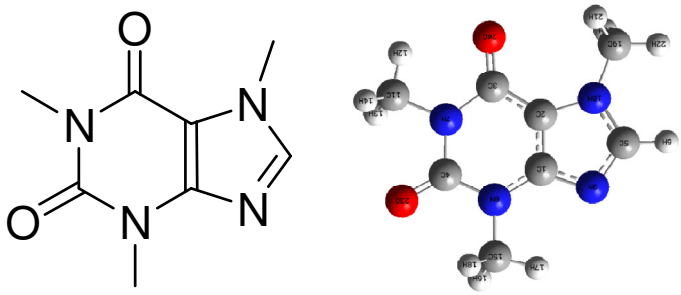

A) **B**)

Figure 7: **A**) Chemical structure used to model Caffeine, **B**) optimized structure of caffeine at B3LYP/6-31G(d) level.

From the figures 6 and 7 above, the optimized structures of ephedrine and caffeine are important for further calculations of their corresponding binding energies to poly (AHNSA).

Optimized Structures of AHNSA-Ephedrine and AHNSA-Caffeine complexes

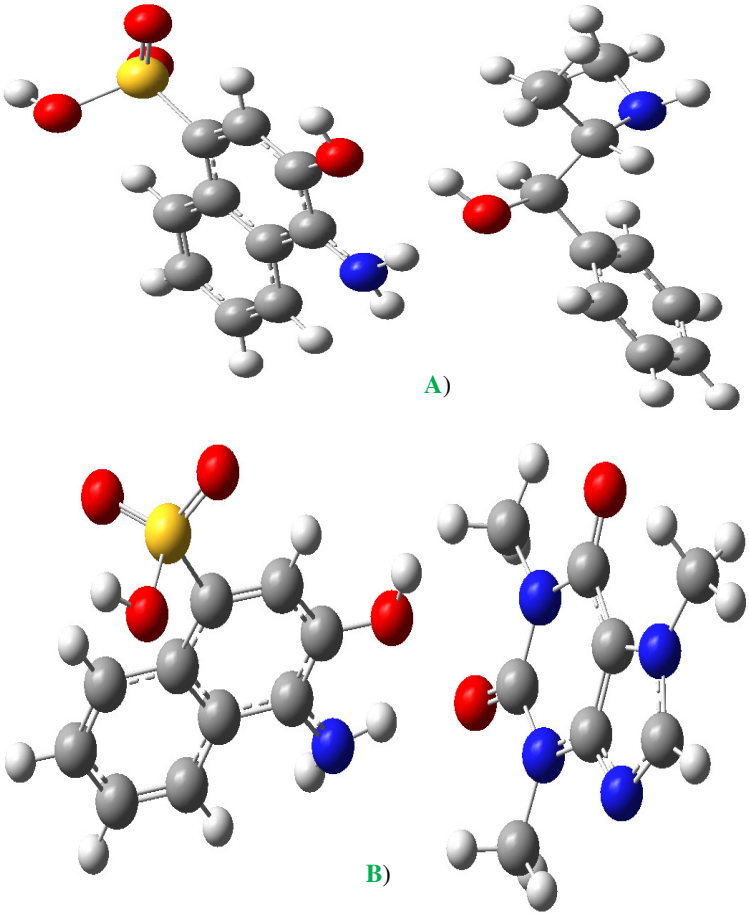

Figure 8: Optimized binding structures of **A**) AHNSA – ephedrine, and **B**) AHNSA - caffeine complexes calculated at B3LYP/6-31G(d).

The binding energies obtained from optimized structures, figures 6, 7, and 8 were presented in the Table 5, to predict the formations of the complexes and to determine their stabilities.

3.6.2 Comparisons of Binding Energies

The binding energy (ΔE) was computed as the difference between the total energy of the complex and the sum of the subsystem energies:

$$\Delta E = E(A-B) - \left[E(A) + E(B)\right]$$

The binding energies of the AHNSA-Ephedrine and AHNSA-Caffeine complexes are given in Table 5.

Table 5: Binding energy values of AHNSA, Ephedrine, Caffeine, AHNSA-Ephedrine complex and AHNSA -Caffeine complexes calculated at B3LYP/6-31G(d) level

$E_{Compound}$	Energy (a.u*)	Energy (kcal mol^{-1})
E_{AHNSA}	-1140.251	
$E_{phedrine}$	-520.045	
$E_{(AHNSA - Ephedrine)complex}$	-1660.310	
$E_{binding}=E_{complex}-[E_{AHNSA}+E_{Ephederine}]$	-0.014	-8.77
$E_{caffeine}$	-680.153	
$E_{(AHNSA - Caffeine)\ complex}$	-1820.638	
$E_{binding}=E_{complex}-[E_{AHNSA}+E_{Caffeine}]$	-0.013	-8.36

1a.u* = 1Hartree = 627.509 469 kcal mol^{-1}

The binding energies of AHNSA-Ephedrine complex is -8.77 kcal mol^{-1} and that of AHNSA-Caffeine complex is -8.36 kcal mol^{-1}. The negative value imply that the complexes are likely to be formed, and when formed, are stable.

4. CONCLUSIONS

A computational study of AHNSA was carried out at the B3LYP/6-31G(d) and B3LYP/6-31+G(d) levels. FMO, MEP, spin density and Mulliken charge population analyses were determined and used to investigate the mechanism of polymerization. Polymer formation of AHNSA likely involves coupling between radical cations, a finding confirmed by FMO and MEP studies. Spin density calculation indicates polymerization of AHNSA occurs selectively *via* $-NH_2$ group. Mulliken charge population analysis of AHNSA suggests electrons are removed from the lone pair of nitrogen.

Binding energies calculations show that AHNSA-Ephedrine and AHNSA-Caffeine complexes are likely to be formed, and that the formed complexes are stable. This study supports previously reported experimental results.

5. REFERENCES

1. Y.Zhousheng, H.Guangzhi, L.Yunchun, Z.Jun and Z. Guangchao, *Canadian J. anal Sci and Spectro.*, **2006**, 52: 11.
2. I.A. Koshets, Z.I. Kazantseva and Y.M. Shirshov, *Semiconductor Physics, Quantum Electronics and Optoelectronics.,***2003**, 6: 505.
3. Y.Ohnuki, T.Ohsaka, H.Matsuda and N. Oyama, *J.Electroanal.Chem.,***1983**, 158: 55.
4. A. Volkov, G. Tourillon, P. C. Lacaze and J.E, Dubois. *J. Electroanal.Chem.,***1980**, 115: 279.
5. A. K. Vinjamuri, S.C. Burris and D. B. Dahl, *The Electrochemical Transactions,***2008**,13: 9.
6. A. Reza and M. B. Keivani, *E-J. Chem*, **2006**, 3: 202.
7. B. Hema, B. Vineet, C. Veena, K. Sundeep, Dhawan, *PolymIn*t, **2009**;58: 489.
8. G.C. Marjanovic, M. Trchova, P. Matejka, P. Holler, B. Marjanovic, I. Juranic, *Reactive & Functional Polymers,***2006***,* 66: 1670.
9. G.C. Marjanovic, B.Marjanovi´c, I Jurani´c, Holler, P, J Stejskal, and Trchova *J, Mater Sci Forum.,***2006,** 518: 405.
10. M. Amare and S. Admassie, *Talanta.,***2012**, 93: 122.
11. M. Amare, W. Lakew and S. Admassie, *Anal. Bioanal. Electrochem.,***2011**, 3(4): 365.
12. S. Sebastian, S. Sylvestre, N. Sundaraganesan, M. Amalanathan, S. Ayyapan, K. Oudayakumar, B. Karthikeyan, *Spectrochimica Acta Part A: Molecular and Biomolecular Spectroscopy*., **2013**, 107: 167.
13. M.J. Frisch, G. W. Trucks, H. B. Schlegel, G. E. Scuseria, M. A. Robb, J. R. Cheeseman, G. Scalmani, V. Barone, B. Mennucci, G. A. Petersson, H. Nakatsuji, M. Caricato, X. Li, H. P. Hratchian, A. F. Izmaylov, J. Bloino, G. Zheng, J. L. Sonnenberg, M. Hada, M. Ehara, K. Toyota, R. Fukuda, J. Hasegawa, M. Ishida, T. Nakajima, Y. Honda, O. Kitao, H. Nakai, T. Vreven, J. A. Montgomery, Jr., J. E. Peralta, F. Ogliaro, M. Bearpark, J. J. Heyd, E. Brothers, K. N. Kudin, V. N. Staroverov, R. Kobayashi, J. Normand, K. Raghavachari, A. Rendell, J. C. Burant, S. S. Iyengar, J. Tomasi, M. Cossi, N. Rega, J. M. Millam, M. Klene, J. E. Knox, J. B. Cross, V. Bakken, C. Adamo, J. Jaramillo, R. Gomperts, R. E. Stratmann, O. Yazyev, A. J. Austin, R. Cammi, C. Pomelli, J. W. Ochterski, R. L. Martin, K. Morokuma, V. G. Zakrzewski, G. A. Voth, P. Salvador, J. J. Dannenberg, S. Dapprich, A. D. Daniels, O. Farkas,

Comment [JCS3]: watch spacing in references – check all entries; there should be a space between initials and last names

Comment [JCS4]: Anal.

J. B. Foresman, J. V. Ortiz, J. Cioslowski, and D. J. Fox, Gaussian *09, Revision A.02*, Gaussian, Inc., Wallingford CT, **2009.**

14. *Gauss View5.0.8*., Gaussian Inc., Wallingford, CT 06492, USA.
15. A.D. Becke, *J. Chem. Phys*. **1993**, 5648: 98.
16. C. Lee, W. Yang, R.G. Parr, *Phys. Rev. B,***1988**, 785: 37
17. I.N. Levine, *Quantum Chemistry*, 5th Ed., Prentice –Hall, Inc., New Jersey, **2000.**
18. D.C. Young, *Computational Chemistry: A Practical Guide for Applying Techniques to Real-World Problems,* John Wiley & Sons, New York, **2001**.
19. E.G. Lewars, *Computational Chemistry; Introduction to the Theory and Applications of Molecular and Quantum Mechanics* 2nd Ed. Springer Science & Business Media B.V., **2011**.